

Second Harmonic Generation in Photonic Crystal Cavities in (111)-Oriented GaAs

Sonia Buckley,^{1, a)} Marina Radulaski,¹ Klaus Biermann,² and Jelena Vučković¹

¹⁾*E. L. Ginzton Laboratory, Stanford University, Stanford, CA 94305, U.S.A.*

²⁾*Paul-Drude-Institut für Festkörperelektronik, Hausvogteiplatz 5-7 D-10117, Berlin, Germany*

We demonstrate second harmonic generation at telecommunications wavelengths in photonic crystal cavities in (111)-oriented GaAs. We fabricate 30 photonic crystal structures in both (111)- and (100)- oriented GaAs and observe an increase in generated second harmonic power in the (111) orientation, with the mean power increased by a factor of 3, although there is a large scatter in the measured values. We discuss possible reasons for this increase, in particular the reduced two photon absorption for transverse electric modes in (111) orientation, as well as a potential increase due to improved mode overlap.

PACS numbers: 42.70.Qs, 78.67.Hc, 42.65.Ky

Low mode-volume, high quality (Q) factor optical microcavities are promising for nonlinear optical devices, as they have the potential to reach similar conversion efficiencies to traditional optical cavities, but in significantly more compact devices. In particular, if the optical mode volume becomes small compared to the material nonlinear coherence length, the phase matching condition is replaced by the requirement of large mode overlap between the relevant optical modes¹. This is particularly useful in the case of III-V semiconductors such as GaAs, GaP and InP, as these materials have a very high second order nonlinearity, but do not exhibit birefringence. This makes phasematching of bulk III-V semiconductors challenging, and typically quasi-phasematching or additional birefringent materials are employed. Quasi-phasematching these materials poses additional challenges as, unlike frequently used LiNbO₃, III-Vs are not ferroelectric and require wafer bonding or epitaxial growth for periodic poling². Conversely, integration of III-V materials with optical microcavities is relatively easy due to the ease of fabrication using semiconductor processing. III-V semiconductors also allow integration of active gain media such as quantum dots or quantum wells³⁻⁵, as well as potential on-chip integration with detectors, switches and modulators.

Experimentally, high efficiency, low power $\chi^{(2)}$ nonlinear processes in resonant microcavities have been demonstrated, in particular second harmonic generation in microdisks⁶ and microrings⁷, as well as second harmonic generation and sum frequency generation in photonic crystal cavities⁸⁻¹⁰. Millimeter sized lithium niobate microdisks have also been used for high efficiency second harmonic generation and ultra-low threshold optical parametric oscillators (OPOs)¹¹⁻¹³. The efficiency of the conversion process is proportional to the quality factors and spatial overlap integral of the three modes involved^{1,14}. In the case of second harmonic generation in photonic crystal cavities, the experimentally achieved ef-

iciency of the processes has been limited by the difficulty of engineering multiple high quality factor modes with a high degree of overlap⁸⁻¹⁰. This difficulty arises because the bandgap of photonic crystals does not span a sufficiently large frequency range for $\chi^{(2)}$ processes, and there are no significant higher order bandgaps. This means that only one of the modes of the photonic crystal cavity in the process is well defined and has high Q. For example, in experimentally demonstrated second harmonic generation in three hole defect (L3) photonic crystal cavities, the pump is coupled to the high Q fundamental cavity mode. Previous work indicates that second harmonic generation in photonic crystal cavities is primarily due to the bulk $\chi^{(2)}$ rather than a surface $\chi^{(2)}$ effect (even in materials where the generated second harmonic is above the bandgap and absorbed,)^{8,9}. This suggests that the second harmonic couples to leaky air band modes perturbed by the presence of the cavity^{4,8-10}, which have low Q factors, and potentially low overlap with the fundamental mode. In order to improve the efficiency, there have been several proposals for designing photonic crystal cavities with multiple high Q resonances and large frequency separations¹⁵⁻¹⁹.

Additional complications in designing nonlinear cavities in III-V semiconductors arise due to the symmetry of the $\chi^{(2)}$ tensor; the only nonzero elements of the bulk $\chi_{ijk}^{(2)}$ have $i \neq j \neq k$, where i, j and k are directions along the [100], [010] and [001] crystal axes. Furthermore, the mode overlap is proportional to $\sum_{ijk} \int dr \chi_{ijk}^{(2)} E_{1i} E_{2j} E_{3k}$, where E is a component of the electric field and the numeric subscript describes a distinct mode in a three wave mixing process. Spatially anti-symmetric products of the three field components have zero overlap. The vertical symmetry of the photonic crystal cavity forces all modes to be either primarily transverse electric (TE) -like or transverse magnetic (TM) -like²⁰. For a TE-like mode, E_x, E_y and H_z obey even symmetry in the vertical direction about the center of the slab while $E_z, H_x, H_y = 0$ at the central xy plane and are anti-symmetric about this plane (where we define z as the direction normal to the wafer, and x and y to be in the plane of the wafer).

^{a)}Electronic mail: bucklesm@stanford.edu.

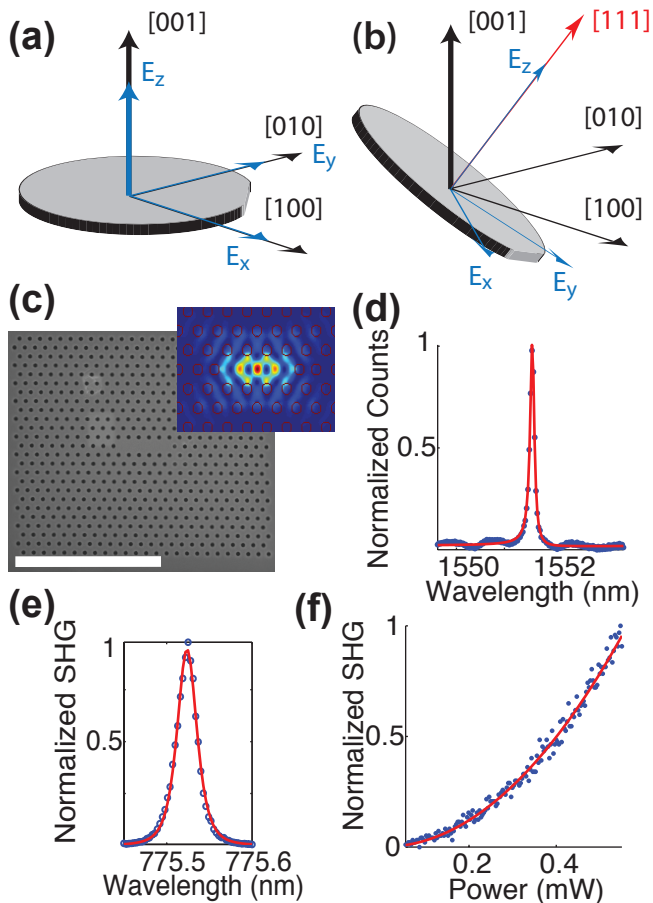


FIG. 1. (a) (001) and (b) (111) oriented III-V semiconductor wafer, showing electric field co-ordinates E_x , E_y and E_z aligned with the crystal axes. For (111) orientation, each field component has components along all three of the main crystal axes. (c) SEM of the three hole defect (L3) photonic crystal cavity fabricated in (111) GaAs. Simulated magnitude of the electric field of the fundamental mode is shown in the inset. Scalebar is $5 \mu\text{m}$. (d) Cross polarized reflectivity spectrum of the cavity in (c) with resonance at 1551 nm . (e) Second harmonic spectrum of the cavity in (c) at $600 \mu\text{W}$ input power. (f) Second harmonic power versus pump power for low pump powers for the same cavity as shown (c)-(e); red line shows quadratic fit.

For TM-like modes, E_z , H_x and H_y obey even symmetry in the vertical direction about the center of the slab while E_x , E_y , $H_z = 0$ at the central xy plane and are anti-symmetric about this plane. Examining the mode overlap integral reveals that for the process of second harmonic generation, a TE-like mode may only couple to a TM-like mode if the wafer is normal to the [100], [010] or [001] (equivalent) directions, as in standard (001) oriented wafers⁹. This is illustrated in Fig. 1 (a). The consequence of this is that both high Q TE-like and TM-like modes must be engineered for second harmonic generation in suspended photonic crystals on this substrate, which is challenging as nearly all planar photonic crystals only have a bandgap for TE polarization (with the

exception of a few recent demonstrations^{21,22}, which require either complex 2D patterns or thick 1D structures, thereby making fabrication more challenging). However, if the wafer is cut such that the plane of the wafer is normal to a different crystallographic direction, the x and y directions in the plane of the wafer may have components along each of the [100], [010] and [001] directions, and in this case TE-TE coupling between modes may be allowed. For example, in the case of (111) oriented III-Vs, illustrated in Fig. 1 (b), such TE-TE mode coupling is allowed. This opens up additional degrees of freedom for engineering photonic crystal cavities for frequency conversion¹⁹, as all three modes in a three wave mixing process may now have either TE-like or TM-like symmetry.

In order to achieve efficient nonlinear frequency conversion, it is also desirable to choose a semiconductor with a transparency window that overlaps well with the experimental frequencies. GaP has a large bandgap and has been demonstrated as a high-efficiency nonlinear source of visible frequencies⁹, but is challenging to grow in (111) orientation. On the other hand, GaAs has a strong nonlinearity, is easier to grow in (111) crystal orientation, and is compatible with bright gain media such as InGaAs quantum wells, and efficient quantum emitters, such as InAs quantum dots^{3,5}. However, GaAs has a smaller bandgap than GaP, and suffers from a large two photon absorption at telecommunications wavelengths, as well as linear absorption of visible wavelengths. Moreover, due to the tensor nature of the nonlinear properties, the two photon absorption of TE modes in (111) GaAs is several times smaller than in (001) GaAs²³.

In order to demonstrate the improvement of nonlinear frequency conversion in nanophotonic structures by controlling the crystal orientation of the underlying material, we fabricate L3 photonic crystal cavities in (001) and (111) GaAs and compare second harmonic generation in both. Photonic crystal cavities were fabricated in 165 nm thick (001) and (111) GaAs membranes grown on a thick AlGaAs sacrificial layer ($1 \mu\text{m}$ thick in the (001) sample, $0.8 \mu\text{m}$ thick in the (111) sample) on n-type doped substrates. The (111)B GaAs substrate was off-oriented by 2° towards [2-1-1]. The cavities were fabricated using e-beam lithography to define the pattern, followed by dry etching and HF wet etching to remove the sacrificial layer. An SEM of a fabricated device is shown in Fig. 1 (c). The fabricated structures had lattice constant $a = 460\text{-}470 \text{ nm}$ and hole radius $r/a = 0.28$. The electric field of the fundamental mode of this cavity is shown inset in the figure, and was simulated by 3D finite difference time domain (FDTD) method. Fabricated photonic crystal cavities were all characterized experimentally at the fundamental (1st harmonic) wavelength with a broadband LED light source using a cross polarized reflectivity method²⁴. The spectrum for the structure shown in Fig. 1 (c), measured by this method, is shown in Fig. 1 (d) with a Q factor of 10,000.

To perform second harmonic generation, a tunable CW

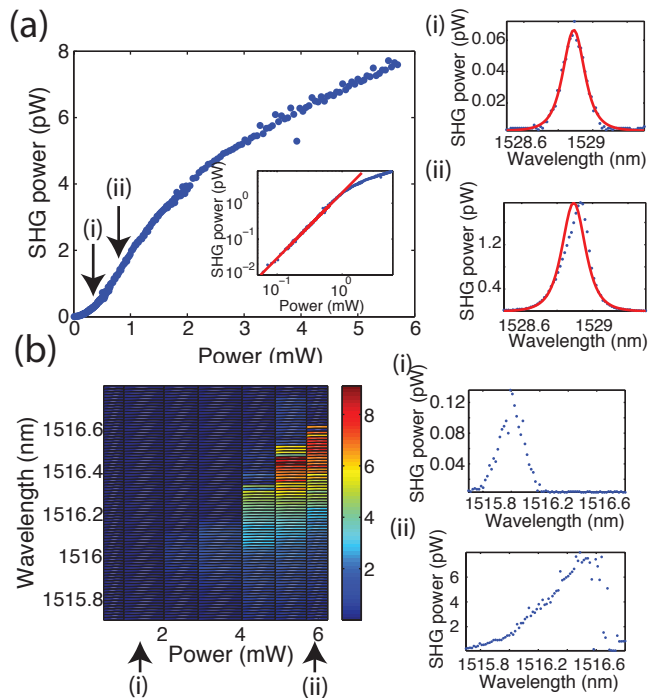


FIG. 2. (a) Second harmonic generation in (111)-GaAs photonic crystal cavities versus input power. Quadratic dependence shown inset on loglog plot. Power versus wavelength at different power levels shown in (i) and (ii). (b) Second harmonic counts versus power versus wavelength for a different structure. (i) and (ii) show the power versus wavelength for two different pump power levels.

telecommunications wavelength (1465-1575 nm) laser is reflected from a 50-50 beamsplitter and coupled to the high-Q fundamental cavity mode at normal incidence with a high numerical aperture objective lens. The second harmonic emission is collected through the same objective and passes through the beamsplitter to be measured on a liquid nitrogen cooled Si CCD spectrometer⁹. The tunable laser is scanned across the cavity resonance, and the maximum counts measured on the spectrometer for each laser wavelength are recorded. The value in counts/second was calibrated in order to calculate actual powers. An example of such a spectrum for the cavity in (111) GaAs measured shown in Fig. 1 (c) at 600 μ W pump power is shown in Fig. 1 (e), the red line is a fit to a Lorentzian squared with Q factor of 10,000. The second harmonic power dependence on input power can be recorded by varying the laser power at a particular wavelength; the resulting curve for the same cavity is shown in part (f), with a quadratic fit in red. Since the generated second harmonic is above the GaAs bandgap, the process efficiency is greatly reduced by the two photon absorption of the pump and linear absorption of the second harmonic; this is indicated by the fact that the measured power is significantly lower than that measured from similar cavities in GaP, despite the relatively higher $\chi^{(2)}$ nonlinearity of GaAs²⁵. Since at low powers the mea-

sured second harmonic versus pump power is quadratic and the efficiency versus pump power is approximately linear, in this power regime we can obtain the (constant) conversion efficiency per Watt of input pump power for each structure. The maximum low power conversion efficiency per Watt measured in a (111)-GaAs structure was 0.002 %/W (not accounting for in/out coupling losses), which is 450 times lower than the measured conversion efficiency per Watt in GaP photonic crystal cavities.

Next, we compare the second harmonic spectra for similar L3 cavities in (111) and (001) GaAs, in order to demonstrate the difference in the second harmonic process in the two orientations for input powers leading to collected second harmonic powers in the pW range. We expect to observe a difference in the measured second harmonic power for fixed pump power, due to differences of the nonlinear optical interaction strengths and of the two-photon absorption coefficients between the two samples, although this experiment will not distinguish between the two effects. Around 30 cavities were fabricated for both (111) and (001) GaAs. The input power was kept at 600 μ W, where the second harmonic generation (SHG) versus pump curve was still quadratic for the case of (111) GaAs, as in Fig. 1 (e), but the power was high enough that second harmonic signal could be measured for most cavities. For (001) GaAs this may have already been in the strong nonlinear absorption regime due to the higher two photon absorption, however, below this power the second harmonic power was too low to measure for a significant number of structures in the (001) orientation, and therefore we chose to measure at 600 μ W in order to keep these structures in our sample. We therefore do not quote low power conversion efficiency for both but rather measure second harmonic power at 600 μ W. For each photonic crystal cavity, the tunable laser was scanned across the resonance. Second harmonic power was plotted versus wavelength, and the peak value was recorded. Table 1 summarizes the results, which indicate higher efficiency SHG in the (111) orientation. A large structure to structure variation was observed, and is possibly due to the high sensitivity of air band mode frequencies to structure parameters, as well as variations in in- and out-coupling efficiency. In order to try to suppress this variation, we also fabricated perturbed L3 photonic crystal cavities²⁶. However, we still observed significant scattering of values. Since this scattering was less severe in the case of GaP cavities in previous studies⁹ (e.g. allowing a noticeable dependence on in plane cavity rotation), we suggest that the absorption contributes to the high sensitivity of measured powers. The results for (001)-oriented GaAs are statistically enhanced by the fact that there were several cavities in that orientation for which we could not measure any SHG, perhaps because the efficiency was too low, and these were not included in the results. Different rotations relative to the crystal axes were also fabricated, however, the variation from structure to structure was larger than any rotation variation that we could measure. Therefore, we include structures

TABLE I. Comparison of second harmonic power in pW for L3 cavities in (001) and (111) GaAs for 600 μ W input power.

	(001) GaAs (pW)	(111) GaAs (pW)
max	1.66	7.3
mean	0.47	1.55
median	0.11	1.03
standard deviation	0.55	1.6

of all rotations in the table. The quality factor of the structures measured was between 8,000 and 13,000, and no significant dependence on Q factor was found in this range. We attribute this to the fact that although the conversion efficiency increases with increase in Q factor, the coupling efficiency decreases with increasing Q factor, and in this range the two effects cancel. The increase in the SHG in (111) cavities relative to (001) cavities may be a combination of the smaller two-photon absorption in (111) GaAs and the possible better overlap between the fundamental L3 cavity mode and air band modes, due to the possibility of coupling to TE modes, as explained above. FDTD simulations of the potential contributing air band modes⁴ were used for calculations of the mode overlap, and indicate that this overlap can be improved or reduced with a change in wafer orientation by up to an order of magnitude, depending on the particular air band modes involved. Determination of which of these modes is involved is challenging, as these modes are low Q and therefore difficult to isolate via FDTD simulation, and in general confirmation via farfield measurements and rotation of the wafer are required. In these simulations however, linear and nonlinear absorption were not included, and therefore identification of the precise modes involved was not possible. Another potential difference is the difference in outcoupling between TE and TM modes. One might naively expect that TM modes would couple out more poorly than the TE modes. However, for the low Q air band modes we simulated (see reference⁴ for an example of such modes), we found that between 20-70 % of the light couples into the NA of the objective lens for both TE modes and TM modes, with more variation depending on the precise mode than between TE and TM. A precise characterization of the improvement resulting from the chosen wafer orientation would require further experiments at longer pump wavelengths to distinguish between improvement from lower two photon absorption and improved overlap due to TE-TE mode coupling.

At higher input pump powers, the generated second harmonic will deviate from a quadratic dependence due to absorption processes and resonance shifts. This is shown in Fig. 2 (a). The fundamental is absorbed via two photon absorption, while the second harmonic is ab-

sorbed linearly. This absorption leads to the generation of free carriers and free carrier absorption. Additionally, free carrier absorption causes a change in refractive index causing the cavity to blueshift²⁷, as well as heating of the cavity, causing the cavity to redshift (microsecond timescale). These transient effects cause regenerative oscillations or bistability, particularly on the red side of the resonance²⁸⁻³⁰, and are of interest for switching and optical signal processing applications^{26,31-33}. In addition, photo-oxidation of the cavity causes a slow and permanent blueshift of the cavity resonance by up to several nm³⁴. The input powers at which this deviation from quadratic behavior occurs varied significantly from cavity to cavity. The described resonance shifts can cause problems during measurement, as high Q cavities shift off resonance suddenly. Fig. 2 (a) parts (i) and (ii) show the second harmonic spectrum at low and higher power; at higher powers the spectrum can be seen to be slightly ‘tilted’ from the Lorentzian squared fit due to nonlinear absorption effects. Fig. 2 (b) shows the second harmonic power versus wavelength versus input power for another cavity with higher absorption. As the power is increased, the spectrum deviates more and more from a Lorentzian squared. This is shown in parts (i) and (ii) where the spectra are shown at the low and high power ends. The high power spectrum is highly asymmetric and the peak has redshifted; the second harmonic also becomes bistable at this side of the spectrum (see supplement).

In summary, we have demonstrated second harmonic generation in (111) GaAs with the pump at telecommunications wavelengths. We observed higher conversion efficiencies for the (111) GaAs than in (001) GaAs, which is most likely due to the combination of reduced two photon absorption for TE-like modes relative to (001) GaAs, and better overlap between involved (TE-like) modes. Future experiments at longer pump wavelengths could assert which effects are more responsible for this difference.

This work was supported by the National Science Foundation (NSF Grant ECCS- 10 25811), a National Science Graduate Fellowship, and Stanford Graduate Fellowships. This work was performed in part at the Stanford Nanofabrication Facility of NNIN supported by the National Science Foundation under Grant No. ECS-9731293, and at the Stanford Nano Center. JV also thanks the Alexander von Humboldt Foundation for support.

SUPPLEMENTARY INFORMATION

To more easily characterize the bistable behavior of the cavities, we fabricated perturbed L3 cavities in both (001) and (111) oriented wafers. An SEM of a perturbed cavity is shown in Fig. 3 (a), the perturbation is an increase in the radius of specific holes in the cavity region

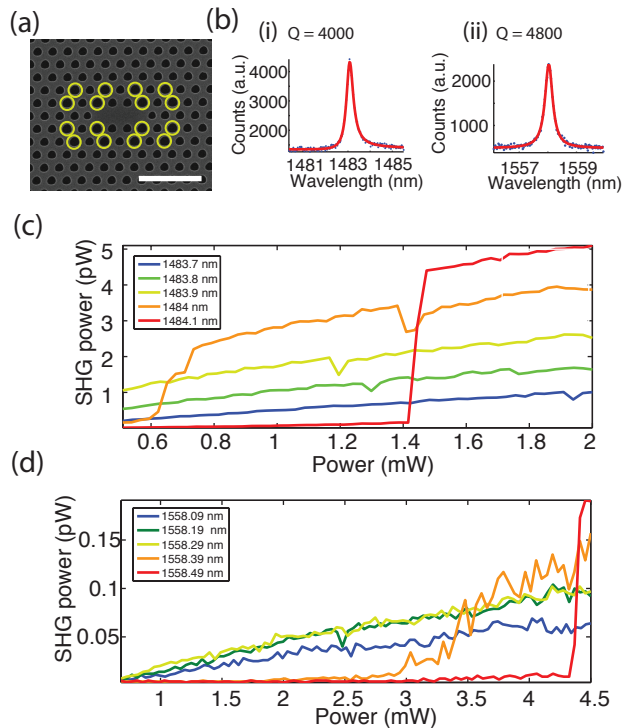


FIG. 3. (a) An SEM of a perturbed L3 cavity, enlarged holes are circled in yellow. The scalebar is $2 \mu\text{m}$. (b) Cross-polarized reflectivity for a perturbed L3 cavity in (i) (111) GaAs and (ii) (001) GaAs. (c)-(d) SHG power versus pump power for different wavelengths for (c) the (111) GaAs cavity characterized in (b) part (i), and (d) the (001) GaAs cavity characterized in (b) part (ii).

indicated by the yellow circles. Incoupling is improved in these cavities by folding back Fourier components outside the light cone to $k = 0$ using a perturbation of period $2a$, where a is the lattice constant. This degrades the Q factor; the cavities we measured had Q factors of 3,000-6,000. Fig. 3 (b) shows cross-polarized reflectivity spectra for cavities in (i) (111) GaAs and (ii) (001) GaAs, with Q factors of 4000 and 4800 respectively. The bistable behaviour was more easily characterized in these cavities. Fig. 3 shows the SHG power versus input power at different wavelengths for a typical perturbed cavity in (c) (111) GaAs and (d) (001) GaAs. These are taken at a power level where the dependence on power is no longer quadratic. The curves shown on the blue side of the resonance are continuous, while the curves on the red side of the resonance have a sudden jump in output power; this jump corresponds to the onset of bistability in the structure. Oscillations will occur at these wavelengths until photo-oxidation blueshifts the resonance far enough and the power becomes unrecoverable. This happens as the cavity heats up and the resonance redshifts and comes into resonance with the laser wavelength. We note that the (001) cavity has lower counts than the (111) cavity at all powers, which was typically the case.

- ¹A. Rodriguez, M. Soljačić, J. D. Joannopoulos, and S. G. Johnson, *Optics Express* **15**, 7303 (2007).
- ²L. A. Eyres, P. J. Tourreau, T. J. Pinguet, C. B. Ebert, J. S. Harris, M. M. Fejer, L. Becouarn, B. Gerard, and E. Lallier, *Applied Physics Letters* **79**, 904 (2001).
- ³K. Rivoire, S. Buckley, A. Majumdar, H. Kim, P. Petroff, and J. Vučković, *Applied Physics Letters* **98**, 083105 (2011).
- ⁴S. Buckley, K. Rivoire, F. Hatami, and J. Vučković, *Applied Physics Letters* **101**, 161116 (2012).
- ⁵Y. Ota, K. Watanabe, S. Iwamoto, and Y. Arakawa, *Optics Express* **21**, 19778 (2013).
- ⁶P. S. Kuo and G. S. Solomon, arXiv:1210.1984 (2012).
- ⁷J. S. Levy, M. A. Foster, A. L. Gaeta, and M. Lipson, *Optics Express* **19**, 11415 (2011).
- ⁸M. W. McCutcheon, J. F. Young, G. W. Rieger, D. Dalacu, S. Frédéric, P. J. Poole, and R. L. Williams, *Physical Review B* **76**, 245104 (2007).
- ⁹K. Rivoire, Z. Lin, F. Hatami, W. T. Masselink, and J. Vučković, *Optics Express* **17**, 22609 (2009).
- ¹⁰S. Diziain, R. Geiss, M. Zilk, F. Schrepel, E.-B. Kley, A. Tünnermann, and T. Pertsch, *Applied Physics Letters* **103**, 051117 (2013).
- ¹¹V. S. Ilchenko, A. B. Matsko, A. A. Savchenkov, and L. Maleki, *Journal of the Optical Society of America B* **20**, 1304 (2003).
- ¹²J. U. Fürst, D. V. Strelakov, D. Elser, M. Lassen, U. L. Andersen, C. Marquardt, and G. Leuchs, *Physical Review Letters* **104**, 153901 (2010).
- ¹³M. Förtsch, J. U. Fürst, C. Wittmann, D. Strelakov, A. Aiello, M. V. Chekhova, C. Silberhorn, G. Leuchs, and C. Marquardt, *Nature Communications* **4**, 1818 (2013).
- ¹⁴M. Liscidini and L. C. Andreani, *Applied Physics Letters* **85**, 1883 (2004).
- ¹⁵Y. Zhang, M. W. McCutcheon, I. B. Burgess, and M. Lončar, *Optics Letters* **34**, 2694 (2009).
- ¹⁶I. B. Burgess, Y. Zhang, M. W. McCutcheon, A. W. Rodriguez, J. Bravo-Abad, S. G. Johnson, and M. Loncar, *Optics Express* **17**, 20099 (2009).
- ¹⁷S. M. Thon, W. T. M. Irvine, D. Kleckner, and D. Bouwmeester, *Physical Review Letters* **104**, 243901 (2010).
- ¹⁸K. Rivoire, S. Buckley, and J. Vučković, *Optics Express* **19**, 22198 (2011).
- ¹⁹K. Rivoire, S. Buckley, and J. Vučković, *Applied Physics Letters* **99**, 013114 (2011).
- ²⁰J. D. Joannopoulos, S. G. Johnson, J. N. Winn, and R. D. Meade, *Photonic Crystals: Molding the Flow of Light (Second Edition)* (Princeton University Press, Princeton, 2011).
- ²¹S.-i. Takayama, H. Kitagawa, Y. Tanaka, T. Asano, and S. Noda, *Applied Physics Letters* **87**, 061107 (2005).
- ²²M. W. McCutcheon, P. B. Deotare, Y. Zhang, and M. Lonar, *Applied Physics Letters* **98**, 111117 (2011).
- ²³M. Dvorak, W. Schroeder, D. Andersen, A. L. Smirl, and B. Wherrett, *IEEE Journal of Quantum Electronics* **30**, 256 (1994).
- ²⁴H. Altug and J. Vuckovic, *Optics Express* **13**, 8819 (2005).
- ²⁵I. Shoji, T. Kondo, A. Kitamoto, M. Shirane, and R. Ito, *Journal of the Optical Society of America B* **14**, 2268 (1997).
- ²⁶See supplementary material at [URL will be inserted by APL] for information on measurements of second harmonic generation in perturbed L3 photonic crystal cavities.
- ²⁷B. Bennett, R. A. Soref, and J. del Alamo, *IEEE Journal of Quantum Electronics* **26**, 113 (1990).
- ²⁸H. M. Gibbs, in *Optical Bistability: Controlling Light with Light* (Academic Press, 1985) pp. 241-303.
- ²⁹V. Van, T. Ibrahim, P. Absil, F. Johnson, R. Grover, and P.-T. Ho, *IEEE Journal of Selected Topics in Quantum Electronics* **8**, 705 (2002).
- ³⁰Q. Xu and M. Lipson, *Optics Letters* **31**, 341 (2006).
- ³¹V. R. Almeida, C. A. Barrios, R. R. Panepucci, and M. Lipson, *Nature* **431**, 1081 (2004).

- ³²K. Nozaki, T. Tanabe, A. Shinya, S. Matsuo, T. Sato, H. Taniyama, and M. Notomi, *Nature Photonics* **4**, 477 (2010).
- ³³L. Fan, J. Wang, L. T. Varghese, H. Shen, B. Niu, Y. Xuan, A. M. Weiner, and M. Qi, *Science* **335**, 447 (2012), PMID: 22194410.
- ³⁴H. S. Lee, S. Kiravittaya, S. Kumar, J. D. Plumhof, L. Balet, L. H. Li, M. Francardi, A. Gerardino, A. Fiore, A. Rastelli, and O. G. Schmidt, *Applied Physics Letters* **95**, 191109 (2009)